

Washington University School of Medicine

Digital Commons@Becker

2020-Current year OA Pubs

Open Access Publications

7-15-2022

17q21.31 sub-haplotypes underlying H1-associated risk for Parkinson's disease are associated with LRRC37A/2 expression in astrocytes

Kathryn R Bowles

Celeste M Karch

et al.

Follow this and additional works at: https://digitalcommons.wustl.edu/oa_4

 Part of the [Medicine and Health Sciences Commons](#)


Please let us know how this document benefits you.

RESEARCH ARTICLE

Open Access



17q21.31 sub-haplotypes underlying H1-associated risk for Parkinson's disease are associated with *LRR37A/2* expression in astrocytes

Kathryn R. Bowles^{1,2} , Derian A. Pugh^{1,2}, Yiyuan Liu^{1,2}, Tulsi Patel^{1,2}, Alan E. Renton^{1,2}, Sara Bandres-Ciga³, Ziv Gan-Or^{4,5,6}, Peter Heutink^{7,8}, Ari Siitonen^{9,10}, Sarah Bertelsen^{1,2}, Jonathan D. Cherry^{11,12,13,14}, Celeste M. Karch¹⁵, Steven J. Frucht¹⁶, Brian H. Kopell^{17,18}, Inga Peter^{19,20}, Y. J. Park^{17,21}, International Parkinson's Disease Genomics Consortium (IPDGC)²², Alexander Charney^{1,17,19,21}, Towfique Raj^{1,2,19,23}, John F. Crary^{1,2,24} and A. M. Goate^{1,2,19,23*}

Abstract

Background: Parkinson's disease (PD) is genetically associated with the H1 haplotype of the *MAPT* 17q21.31 locus, although the causal gene and variants underlying this association have not been identified.

Methods: To better understand the genetic contribution of this region to PD and to identify novel mechanisms conferring risk for the disease, we fine-mapped the 17q21.31 locus by constructing discrete haplotype blocks from genetic data. We used digital PCR to assess copy number variation associated with PD-associated blocks, and used human brain postmortem RNA-seq data to identify candidate genes that were then further investigated using in vitro models and human brain tissue.

Results: We identified three novel H1 sub-haplotype blocks across the 17q21.31 locus associated with PD risk. Protective sub-haplotypes were associated with increased *LRR37A/2* copy number and expression in human brain tissue. We found that *LRR37A/2* is a membrane-associated protein that plays a role in cellular migration, chemotaxis and astroglial inflammation. In human substantia nigra, *LRR37A/2* was primarily expressed in astrocytes, interacted directly with soluble α -synuclein, and co-localized with Lewy bodies in PD brain tissue.

Conclusion: These data indicate that a novel candidate gene, *LRR37A/2*, contributes to the association between the 17q21.31 locus and PD via its interaction with α -synuclein and its effects on astrocytic function and inflammatory response. These data are the first to associate the genetic association at the 17q21.31 locus with PD pathology, and highlight the importance of variation at the 17q21.31 locus in the regulation of multiple genes other than *MAPT* and *KANSL1*, as well as its relevance to non-neuronal cell types.

Keywords: 17q21.31, Parkinson's disease, *LRR37A*, Copy number variation, Astrocytes

Background

The *MAPT* 17q21.31 locus lies within a 1.5 Mb inversion region of high linkage disequilibrium (LD), conferring two distinct haplotypes; H1, which has a frequency of ~0.8 in European ancestry populations, and the less

*Correspondence: alison.goate@mssm.edu

¹ Department of Genetics and Genomic Sciences, Icahn School of Medicine at Mount Sinai, New York, NY, USA
Full list of author information is available at the end of the article



© The Author(s) 2022. **Open Access** This article is licensed under a Creative Commons Attribution 4.0 International License, which permits use, sharing, adaptation, distribution and reproduction in any medium or format, as long as you give appropriate credit to the original author(s) and the source, provide a link to the Creative Commons licence, and indicate if changes were made. The images or other third party material in this article are included in the article's Creative Commons licence, unless indicated otherwise in a credit line to the material. If material is not included in the article's Creative Commons licence and your intended use is not permitted by statutory regulation or exceeds the permitted use, you will need to obtain permission directly from the copyright holder. To view a copy of this licence, visit <http://creativecommons.org/licenses/by/4.0/>. The Creative Commons Public Domain Dedication waiver (<http://creativecommons.org/publicdomain/zero/1.0/>) applies to the data made available in this article, unless otherwise stated in a credit line to the data.

common, inverted H2 haplotype (frequency ~0.2), which is absent or lower frequency in East and South Asian populations (frequency 0–0.09) (Fig. 1A). The major haplotype, H1, has been genetically associated with increased risk for multiple neurodegenerative disorders, including *APOE* ϵ 4-negative Alzheimer's disease (AD) [1], corticobasal degeneration (CBD) [2], progressive supranuclear palsy (PSP) [3–5] and Parkinson's disease (PD) [6–10].

PD is a movement disorder that commonly involves executive dysfunction and dementia [11, 12], but is classically characterized by bradykinesia, tremor, rigidity, postural instability, and numerous non-motor symptoms [13]. Neuropathologically, PD is an α -synucleinopathy defined by the presence of intraneuronal accumulation of α -synuclein in Lewy bodies throughout the substantia nigra, brainstem and forebrain [14, 15]. Despite the genetic association with the 17q21.31 *MAPT*/tau locus, aggregated tau is not a typical neuropathological feature of PD [15], although it is not rare for tauopathy to occur alongside α -synuclein inclusions in the substantia nigra [16, 17]. There is also no apparent association between PD and the H1c sub-haplotype [18, 19], which is strongly associated with risk for the primary tauopathies PSP and CBD [2, 3], indicating that different 17q21.31 locus variants and mechanisms may underlie the relative risk for each disease. Indeed, the 17q21.31 locus spans 1.5 Mb including multiple genes in addition to *MAPT*, and comprises several sub-haplotypes, defined by complex rearrangements and copy number variation in their distal regions [20, 21], the functional impact of which has not yet been explored. Indicative of this complexity, the 17q21.31 locus is genetically associated with many different phenotypes in addition to neurodegenerative diseases, the mechanisms for which remain largely unknown.

Given the specific loss of midbrain dopaminergic neurons in PD, this cell type has been the main focus of efforts to understand the mechanism of neuronal loss. Similarly, investigation of 17q21.31 variants is also often restricted to neurons, due to the high neuronal expression of *MAPT*. However, a causal role for astrocytes in PD pathogenesis has been recently proposed [22–25]. Indeed, many PD-associated genes are expressed in

astrocytes and have known functional roles in astrocyte biology [24]. Furthermore, α -synuclein-positive aggregates have been identified in the cytoplasm of astrocytes in PD [26–28], indicating aberrant protein accumulation occurring as a result of either neuronal-glia transmission [22, 28, 29], or increased expression of endogenous α -synuclein in astrocytes themselves [25].

Although PD, like PSP and CBD, is associated with the H1 haplotype, the odds ratio for risk is substantially lower (1.5 vs 4.5) in PD [2–10]. Furthermore, in contrast to PSP and CBD, PD has not been associated with the H1c sub-haplotype [18, 19] and is not generally associated with the accumulation of tau. Together these observations suggest that the PD genetic association with the 17q21.31 locus may be driven by genes other than *MAPT*. Here, we report three sub-haplotype blocks associated with PD risk within the 17q21.31 H1 haplotype clade, with both protective and risk-associated sub-haplotypes within each block. We show that protective sub-haplotypes are associated with increased expression and copy number of *LRR37A/2*, which we demonstrate is an astrocyte-enriched membrane-associated protein with a role in chemotaxis and the inflammatory response, and co-localizes with both soluble α -synuclein and Lewy bodies in human substantia nigra. These findings link the genetic association at the 17q21.31 locus with PD pathology, and support the hypothesis of astroglial dysfunction as a key contributing factor to PD disease pathogenesis.

Results

PD risk is associated with the 17q21.31 H1 haplotype

To confirm the genetic association of the 17q21.31 H1 haplotype with PD risk in our specific cohorts, we carried out a case–control association analysis across the region of interest (Figure S1A–E, Table S1) in two independent datasets (Stage 1 2,780 PD cases, 6,384 controls; Stage 2 2,699 cases, 2,230 controls; Table S2). The SNP with the strongest association in Stage 1 (rs17763050, $p=2.74 \times 10^{-9}$) was in high LD with the known H1/H2 haplotype tag SNP rs8070723 ($D'=0.98$, Figure S1B–C, F). Both SNPs were associated with odds ratios (ORs) ~0.8 (95% CI ± 0.1 ; Figure S1B–C, Table S1), consistent with previously reported effect sizes^{6,8}. Due to a smaller cohort size and consequent lack of power, the

(See figure on next page.)

Fig. 1 H1 sub-haplotypes within the *MAPT* 17q21.21 inversion region are associated with Parkinson's disease risk. **A.** Structure of the 17q21.31 locus, which confers two distinct sub-haplotypes defined by gross structural inversion; H1 and H2. Direction of gene orientation in each haplotype is indicated by arrows. Each gene or partial gene is labeled with a distinct color and connected with a crossed rectangle between H1 and H2 to aid visualization of altered gene position between haplotypes. **B–C.** H1 sub-haplotype block association ($-\log_{10} p$ -value) with PD plotted above H1 homozygote D' LD structure and sub-haplotype blocks generated from **B.** Stage 1 data and **C.** Stage 2 data, spanning Hg19 Chr17:43,384,997–44,913,630. **C.** Association ($-\log_{10} p$ -value) of blocks calculated in Stage 2 data (blue, top), and H1.1, H1.2 and H1.3 blocks as defined in Stage 1 applied to Stage 2 data (orange, bottom). In LD plots, red indicates high D' and blue indicates low. Black arrows indicate similar blocks generated across Stage 1 and Stage 2 data. Grey lines indicate genome wide suggestive significance p -value of 1×10^{-5}

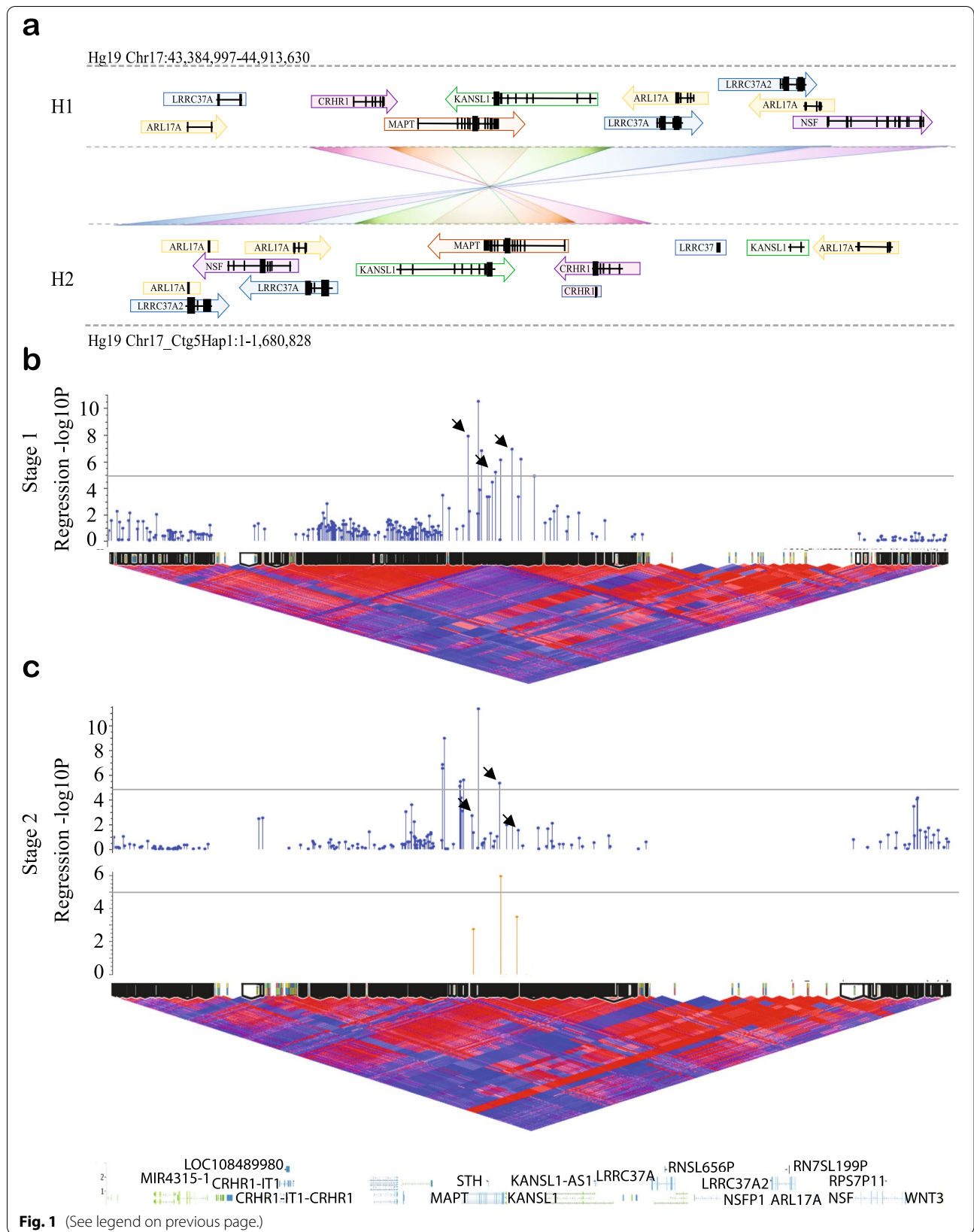


Table 1 17q21.31 H1 sub-haplotype blocks associated with PD susceptibility

Block	#Sub-haplotypes	#SNPs	Start	Stop	Gene	Location	Stage 1			Stage 2		
							p-value	-log ₁₀ p-value	FDR p-value	p-value	-log ₁₀ p-value	FDR p-value
H1.1	5	5	44,040,184	44,041,992	MAPT	Intronic	1.35E-08	7.87	1.73E-06	1.94E-03	2.71	4.50E-03
H1.2	8	8	44,090,196	44,097,249	MAPT	Intronic/Exonic	6.58E-06	5.18	2.40E-04	1.12E-09	5.95	7.84E-06
H1.3	7	9	44,119,987	44,131,305	KANSL1	Intronic	1.23E-07	6.91	1.05E-05	2.39E-04	3.47	1.12E-03

association with 17q21.31 was less prominent in Stage 2 data (Figure S1D-E, Table S1), and the top SNP did not tag the H2 haplotype. However, meta-analysis of both cohorts confirmed a significant association between PD risk and the 17q21.31 locus (Figure S1B-C, Table S1), with the H2 haplotype conferring protection (OR 0.82 (95% CI 0.76–0.89)) and the H1 haplotype therefore associated with increased risk.

As the major H1 haplotype was associated with increased risk for PD, we repeated the association analysis in H1 homozygotes alone in order to identify variants of H1 that may confer additional risk for PD (Figure S1G-J, Table S1). While association across the 17q21.31 locus was weaker in H1 homozygotes compared to the full data set, we observed a distinct signal spanning *MAPT* and *KANSL1* in Stage 1 and Stage 2 analyses (Figure S1G-H). The Stage 1 top SNP, rs41543512, was associated with an OR of 1.21 (95% CI 1.10–1.32, $p < 0.001$; Figure S1I, Table S1), but did not reach statistical significance in Stage 2 data or meta-analysis (Table S1). The most significant SNP in the Stage 2 analysis (rs139217062) was not present in Stage 1 data, although the second most significant variant from Stage 2, rs16940711, was not significant in Stage 1 data or by meta-analysis (Table S1, Figure S1J). These data suggest that the H1 association with PD may be more complex than variation in individual SNPs.

17q21.31 H1 sub-haplotype blocks spanning *MAPT* & *KANSL1* are associated with PD risk

As SNP-based association analyses were unsuccessful in identifying significant H1 sub-haplotypic variants contributing to PD risk, we decided to leverage the presence of high linkage disequilibrium (LD) within this region to investigate sub-haplotype blocks. We calculated discrete sub-haplotype blocks spanning the 17q21.31 locus using the D' measure of LD, and performed a logistic regression association analysis on each block (Fig. 1B-C, Table 1). This approach greatly improved the power to detect disease-associated H1 variants in both Stage 1 and Stage 2 data. In Stage 1, we observed a peak spanning *MAPT* and the first 5 exons of *KANSL1* (Fig. 1B) that reached the genome-wide suggestive significance threshold of $p = 1 \times 10^{-5}$. Within this peak, three sub-haplotype blocks showed substantial overlap of SNPs in independently calculated blocks in Stage 2 data (Stage 1 blocks H1.1 ($p = 1.73 \times 10^{-6}$), H1.2 ($p = 2.4 \times 10^{-4}$) and H1.3 ($p = 1.05 \times 10^{-5}$); Fig. 1C, Table 1). We then applied the Stage 1-constructed blocks to Stage 2 data and observed replication of their association with PD risk (Fig. 1C, Table 1). Block H1.2 was highly significant in Stage 2 data ($p = 1.12 \times 10^{-9}$), while both blocks H1.1 and H1.3 were nominally significant ($p < 0.002$ and $p < 0.0003$, respectively).

In order to determine whether the sub-haplotype blocks we identified were merely recapitulating previously defined *MAPT* sub-haplotypes [30], we estimated the frequency of each *MAPT* sub-haplotype in Stage 1 data using tag SNPs rs1467967, rs242557, rs3785883, rs2471738 and rs7521. We then overlaid the frequency of these *MAPT* sub-haplotypes with the frequency of each sub-haplotype across blocks H1.1, H1.2 and H1.3 (Figure S1K). We did not see any association between previously defined *MAPT* sub-haplotypes and block sub-haplotypes, although H1c was enriched in, but not exclusive to, protective block sub-haplotypes H1.1c, H1.2b and H1.3b (Figure S1K). Furthermore, there was no significant association between any *MAPT* sub-haplotype and PD risk in these data (Table S3, Figure S1L), indicating that the sub-haplotype blocks we have identified detect variation across the 17q21.31 locus associated with PD risk that are independent of previously defined *MAPT* sub-haplotypes.

Blocks H1.1, H1.2 and H1.3 each consist of multiple SNPs in high LD (Figure S1M) that generate multiple sub-haplotypes (Figure S2A-F). As many SNPs within these blocks were imputed, we confirmed the existence and frequency of each block and sub-haplotype using whole genome sequence (WGS) data from AMP-PD (Table S4, amp-pd.org), with the exception of H1.1d. This sub-haplotype occurred at a higher frequency than identified in Stage 1 data (~ 0.2 vs 0.06 – 0.1), and at an equivalent frequency to Stage 2 data (~ 0.2). Further investigation indicated this discrepancy was a result of skewed frequency of the H1.1d tag SNP rs16940758 in the American (NIH) cohort in Stage 1 data, but occurred at a similar frequency to the WGS data in the other three contributing datasets, suggesting a possible technical or imputation error for this variant. All other variants of interest and sub-haplotypes occurred at a similar frequency across cohorts and WGS data (Table S4), indicating accuracy of imputation and sub-haplotype construction.

Each sub-haplotype was differentially associated with PD susceptibility (Figure S2A,C,E, Table 2), with each block containing both risk- and protective sub-haplotypes with ORs ranging from 0.37 (95% CI 0.32–0.42, $p = 1.3 \times 10^{-49}$, H1.1c) to 2.51 (95% CI 2.2–2.86, $p = 2.4 \times 10^{-45}$, H1.1e). Despite the presence of heterogeneity between Stages 1 and 2, the most frequently occurring sub-haplotypes were replicated in both analysis stages and by fixed effects meta-analysis (Table 2). Specifically, we identified two sub-haplotypes in block H1.1; H1.1b and H1.1e, which increased risk in both datasets when compared against the most common haplotype, with ORs ranging from 1.26–1.6 (fixed effects $p < 0.001$) and 1.45–2.51 (fixed effects $p < 0.001$), respectively (Figure S2A-B, Table 2). In the same block we also observed

Table 2 (continued)

Block ID	Sub-haplotype	Stage 1				Stage 2				Meta				
		Sub-haplotype	Frequency (Case/Control)	OR (95% CI)	OR Fisher's exact p^{sig}	Sub-haplotype	Frequency (Case/Control)	OR (95% CI)	OR Fisher's exact p^{sig}	RE Heterogeneity (p)	RE p^{sig}	FEOR (95% CI)	FE Heterogeneity (p)	FE p^{sig}
H1.3	H1.3a	GACTGA GAT	0.28 (0.32/0.27)	1	-	0.32 (0.32/0.32)	1	-	1	-	1	-	-	-
	H1.3b	CATTAG GGC	0.18 (0.11/0.22)	0.43 (0.38-0.49)	1.66E-41***	0.18 (0.18/0.19)	0.95 (0.81-1.11)	5.22E-01	0.64 (0.29-1.44)	58.53 (<0.00001)	2.80E-01	0.57 (0.52-0.63)	58.57 (<0.0001)	0***
	H1.3c	GATTGA GAT	0.17 (0.21/0.16)	1.11 (0.99-1.24)	7.37E-02	0.16 (0.16/0.17)	0.95 (0.80-1.12)	5.33E-01	1.04 (0.89-1.21)	2.24 (0.134)	6.10E-01	1.06 (0.96-1.16)	2.24 (0.1343)	0.23
	H1.3d	CTTTGG TGC	0.15 (0.12/0.16)	0.61 (0.54-0.7)	1.58E-14***	0.2 (0.21/0.18)	1.16 (0.99-1.36)	5.81E-02	0.84 (0.45-1.56)	35.27 (<0.00001)	5.80E-01	0.77 (0.7-0.85)	35.28 (<0.0001)	2.96E-07***
	H1.3e	CATTGG GGC	0.09 (0.14/0.07)	1.67 (1.45-1.92)	2.79E-13***	0.02 (0.02/0.02)	0.81 (0.54-1.21)	2.83E-01	1.19 (0.58-2.42)	12.01 (0.0004)	6.30E-01	1.54 (1.35-1.75)	12.01 (0.0005)	4.57E-11***
	H1.3f	CATTGG GGT	0.08 (0.07/0.09)	0.6 (0.51-0.70)	9.34E-11***	0.09 (0.1/0.08)	1.15 (0.93-1.42)	2.00E-01	0.81 (0.44-1.5)	21.37 (<0.00001)	5.10E-01	0.74 (0.66-0.84)	21.38 (<0.0001)	3.59E-06***
	H1.3g	GATCGA GAT	0.04 (0.04/0.04)	0.83 (0.67-1.03)	9.39E-02	0.03 (0.02/0.02)	0.55 (0.38-0.78)	5.58E-04***	0.7 (0.49-1.02)	3.48 (0.062)	6.60E-02	0.75 (0.63-0.9)	3.48 (0.062)	1.6E-03**

OR Odds ratio, CI Confidence interval, RE Random effects meta-analysis, FE Fixed effects meta-analysis. * $p < 0.05$, ** $p < 0.01$, *** $p < 0.001$

a protective sub-haplotype (H1.1c), associated with an OR ranging 0.37–0.96 (fixed effects $p < 0.001$; Figure S2A–B, Table 2). Blocks H1.2 and H1.3 encompassed multiple sub-haplotypes with frequencies < 0.1 , and exhibited greater variability and heterogeneity across stages. However, we identified one risk-associated sub-haplotype in block H1.2 (H1.2c, OR = 1.12–1.31, fixed effects $p < 0.01$) and two protective sub-haplotypes in block H1.3 (H1.3b; OR = 0.95–0.43, fixed effects $p < 0.001$, H1.3 g; OR = 0.55–0.83, fixed effects $p < 0.002$; Table 2, Figure S2C–F). These data reflect the variability and complexity present across the 17q21.31 locus, and indicate that numerous H1 variants exist that are associated with differential levels of risk for PD.

PD-associated sub-haplotypes are associated with *LRRC37A/2* gene expression in human brain

In order to elucidate the functional consequences of PD-associated H1 block sub-haplotypes we queried publicly available post-mortem human brain RNA-seq data from dorsolateral prefrontal cortex (PFC) and temporal cortex (TCX) from the AMP-AD and CommonMind consortia (Table S5). Despite the position of the H1 association peaks across *MAPT* and *KANSL1*, we did not observe any differences in the expression of either of these genes between any sub-haplotypes in any block (Fig. 2C, Figure S3A–C). The only genes within the 17q21.31 locus that had a significant association with H1 PD-associated sub-haplotypes were *LRRC37A* and its paralog *LRRC37A2* (a.k.a *LRRC37A/2*; Fig. 2A–B, Figure S3D). We observed significantly increased *LRRC37A/2* expression in protective sub-haplotypes, specifically in H1.1c and H1.3b (H1.1c ~ 4.7 fold, $p < 0.001$, H1.3b ~ fivefold, $p < 0.001$), as well as in sub-haplotypes whose effects were not replicated across PD data-sets; H1.2b and H1.3e (H1.2b ~ 5, $p < 0.001$, H1.3e ~ 2.9x, $p < 0.01$), but were protective in the Stage 2 PD analysis (Fig. 2A–B). qRT-PCR on postmortem prefrontal cortex from a small number of individuals supported the observation of increased *LRRC37A/2* expression in these sub-haplotypes (Figure S3D).

We observed a significant reduction in *LRRC37A/2* expression in the PD risk-associated H1.1b sub-haplotype by qRT-PCR in human brain tissue ($p < 0.01$; Figure S3D), but not in the RNA-seq data. We also did not observe any difference in *MAPT* exons 2, 3 or 10 percent spliced in

(PSI) values between sub-haplotypes (Figure S4A). Interestingly, *LRRC37A/2* expression was significantly higher in the protective 17q21.31 H2 haplotype (Figure S4B), which is consistent with our observation of increased *LRRC37A/2* expression in protective H1 sub-haplotypes. These data suggest that both the 17q21.31 H1/H2 and H1 sub-haplotype genetic associations with PD risk may be due to variable *LRRC37A/2* expression.

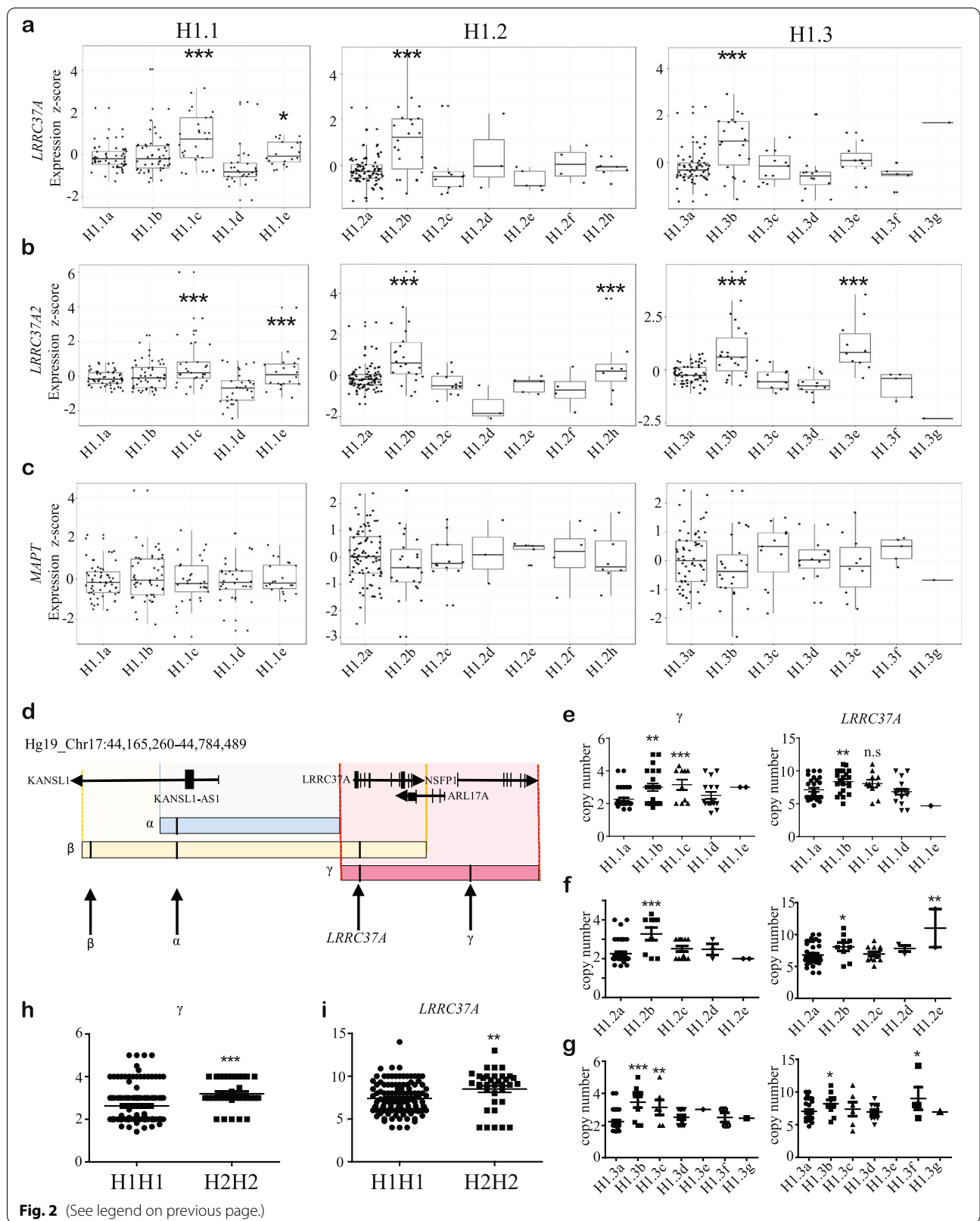
Protective sub-haplotypes are associated with increased *LRRC37A/2* copy number

The 17q21.31 locus is structurally complex and encompasses regions of copy number variation (CNV) at its distal ends [20, 21]. As sub-haplotype blocks within *MAPT* and *KANSL1* were associated with altered *LRRC37A/2* expression, we tested whether they also tagged structural variants [20] in individuals homozygous for sub-haplotypes of interest (Fig. 2D–H, Figure S5A–D). Using DNA derived from either blood or brain tissue (Table S5) we performed digital PCR (dPCR) for *MAPT*, alpha, beta and gamma regions (Fig. 2D) [20], as well as for *LRRC37A/2* specifically (Fig. 2E–G, Figure S5A–D).

The majority of the structural variation in alpha and beta regions were found in the most common sub-haplotype for each block (H1.1a, H1.2a and H1.3a), with each subsequent sub-haplotype carrying fewer copies of these regions (Figure S5A–C). However, gamma and *LRRC37A/2* CNVs varied by sub-haplotype within each block; those sub-haplotypes exhibiting increased *LRRC37A/2* expression were also associated with significantly increased gamma (H1.1c $R^2 = 0.23$, H1.2b $R^2 = 0.25$, H1.3b $R^2 = 0.34$, ~ 3–5 copies compared to 2–3 copies in controls, $p < 0.05$) and/or *LRRC37A/2* copy number (H1.1c $R^2 = 0.06$, H1.2b $R^2 = 0.08$, H1.3b $R^2 = 0.09$, ~ 8–11 copies compared to 5–10 copies in controls, $p < 0.05$; Fig. 2E–G). Interestingly, risk-associated sub-haplotype H1.1b was associated with increased gamma and *LRRC37A/2* copy number ($p < 0.01$; Fig. 2E) but not *LRRC37A/2* expression (Fig. 2A–B), indicating that additional factors likely contribute to *LRRC37A/2* expression and PD risk in this locus, such as chromatin looping or variants within *LRRC37A/2* itself. Consistent with the expression data, we also observed increased beta, gamma and *LRRC37A/2* copy number in H2 homozygotes compared to H1 (Figure S5D). These data suggest that structural variation at the distal end of the

(See figure on next page.)

Fig. 2 PD-associated sub-haplotypes are associated with *LRRC37A/2* expression and copy number **A–C**. Expression of **A.** *LRRC37A*, **B.** *LRRC37A2* and **C.** *MAPT* in human brain tissue, measured by RNA-seq across three different cohorts, split by sub-haplotype in blocks H1.1, H1.2 and H1.3. **D.** Schematic of the regions of copy number variation in the 3' distal end of the 17q21.31 locus, as defined by Boettger et al. 2012 [20]. Black arrows indicate the location of dPCR probes for (left to right) beta, alpha, *LRRC37A* and gamma. **E–G.** Copy number of gamma and *LRRC37A/2* regions in blocks **E.** H1.1, **F.** H1.2 and **G.** H1.3. **H–I.** Copy number of **H.** gamma and **I.** *LRRC37A/2* regions between H1 and H2 homozygotes. All statistical comparisons are against the most common sub-haplotype. ns = not significant, * $p < 0.05$, ** $p < 0.01$, *** $p < 0.001$.



17q21.31 locus may underlie increased expression of *LRRC37A/2* in protective H2 and H1 sub-haplotypes.

LRRC37A is a membrane-associated protein implicated in cellular migration, chemotaxis and inflammation

As PD sub-haplotypes converge on the expression and/or copy number of *LRRC37A/2*, we explored the likely function of this gene. We carried out RNA-seq analysis in HEK293T cells overexpressing *LRRC37A/2* in order to mimic increased copy number and to elucidate a potential function for this gene. The number of significantly differentially expressed protein-coding genes (fold change ± 1.5 , adjusted $p < 0.05$) in the context of *LRRC37A/2* overexpression was minimal (28 upregulated, 21 downregulated), suggesting that *LRRC37A/2* is unlikely to play a major regulatory role. In order to confirm that we were not observing spurious changes in gene expression due to gross overexpression in a cell culture model, we carried out a titration of *LRRC37A/2* overexpression in HEK293T cells. We observed dose-dependent changes in the expression of genes that were significantly up or downregulated in our RNA-seq data (Figure S6A–D), confirming that the expression of these genes is likely to be altered by *LRRC37A/2* expression.

Functional enrichment of gene ontology (GO) terms for significantly differentially expressed genes indicated a role for *LRRC37A/2* at the cell membrane (Fig. 3A–B, Figure S6E–F), which we confirmed by western blot in HEK293T cells (Figure S6G). In addition, *LRRC37A/2* overexpression also resulted in significant enrichment for *cell communication* (GO:0,007,154, $p < 0.05$) and *neuroactive ligand-receptor interaction* (KEGG:04,080, $p < 0.05$) pathways, as well as nominal enrichment for membrane-component-related pathways (Figure S6F).

Ingenuity pathway analysis (IPA) also suggested a role for *LRRC37A/2* at the plasma membrane and in the extracellular space; specifically, these analyses indicated that increased *LRRC37A/2* expression resulted in upregulated cellular movement pathways, such as increased *migration of cells* ($p < 0.01$, z score = 1.85; Fig. 3A) and upregulation of *chemotaxis* ($p < 0.05$, z score = 0.918; Fig. 3B). Several upregulated genes within these pathways are also essential in regulation of the inflammatory response; both *IL17F* and *IL32* are pro-inflammatory cytokines that mediate the inflammatory response of astrocytes [31, 32], whereas *IL16* acts as a chemoattractant for cells expressing CD4. These data therefore suggest that increased *LRRC37A/2* expression may mediate astroglial inflammation and modify cellular migration in response to a stimulant, such as α -synuclein.

LRRC37A/2 is expressed in astrocytes and impacts cellular migration and response to α -synuclein

Our pathway analysis indicated that *LRRC37A/2* is associated with cellular signaling and pro-inflammatory pathways relevant to astroglial function. We therefore sought to confirm whether *LRRC37A/2* was expressed and functional in these cells. As *LRRC37A/2* expression and copy number was higher in 17q21.31 H2 haplotype carriers compared to H1, and due to difficulty in identifying multiple human iPSC lines with specific H1 sub-haplotypes, we compared the expression of *LRRC37A/2* and genes altered by *LRRC37A/2* expression in iPSC-derived neurons and astrocytes homozygous for either H1 or H2 haplotypes in order to identify the most relevant neural cell type (Fig. 3C, Figure S6H). While *LRRC37A/2* was expressed in both cell types, we observed increased expression of *LRRC37A/2* and associated genes in H2

(See figure on next page.)

Fig. 3 *LRRC37A/2* expression is associated with increased cellular migration, chemotaxis and inflammation. **A–B.** Significantly enriched **A.** *Migration of cells* and **B.** *Chemotaxis* pathways associated with *LRRC37A/2* overexpression, derived from Ingenuity pathway analysis. Red genes indicate upregulation, green indicates downregulation **C.** qRT-PCR for *LRRC37A* expression in H1 and H2 homozygote iPSC-derived neurons and astrocytes. $N = 3$ in duplicate. ns = not significant, $*p < 0.05$. **D.** Western blots for *LRRC37A/2* in cytosolic (C) and membrane (M) fractions from (top) iPSC-neurons and (bottom) iPSC-astrocytes. Cytosolic fractions were confirmed by labeling with an anti-HSP90 antibody, and membrane fractions were confirmed by labeling with an anti-Pan-Cadherin antibody, $N = 6$. **E.** Proportion of *LRRC37A/2*-expressing astrocytes by 17q21.31 haplotype from human prefrontal cortex snuc-seq data [33]. Dot size = proportion of cells expressing *LRRC37A/2*, depth of color = *LRRC37A/2* expression level. **F.** Representative immunofluorescence images of iPSC-derived astrocytes expressing either scrambled control or *LRRC37A/2* shRNA lentivirus constructs, labeled with antibodies against either IL-16 or IL-32. Scale bar = 10 μ m. **G.** Quantification of mean grey intensity of astrocytes in immunofluorescence images represented in **F.** Each point represents the average of 12–16 individual images from an individual cell line. Four cell lines were analyzed. Points from the same iPSC line are connected between scrambled and *LRRC37A/2* shRNA conditions. Overall p -value indicates paired t-test of cell line image means. Asterisks denote significant between scrambled and *LRRC37A/2* conditions for each paired line. $*p < 0.05$, $***p < 0.001$, ns = not significant. **H.** Wound confluence (%) of scratch wound repair over 50 h in scrambled control (dashed lines) and *LRRC37A/2* shRNA (solid lines) treated iPSC-derived astrocytes treated with either 200 ng/ml α -synuclein monomers (orange) or PBS (green). Statistical difference between groups over time was determined by ANCOVA and post-hoc Tukey tests. $*p < 0.05$, $***p < 0.001$. $N = 4$. **I.** Representative images with quantification masks of iPSC-astrocytes at 0 h, 16 h and 24 h following induction of a scratch wound in scrambled control (top) and *LRRC37A/2* shRNA (bottom) treated cells, with (right panels) and without (left panels) incubation with 200 ng/ml α -synuclein. Yellow masks indicate cell confluence, blue indicates the scratch wound area, and grey indicates cellular migration into the original wound area. Scale bar = 600 μ m

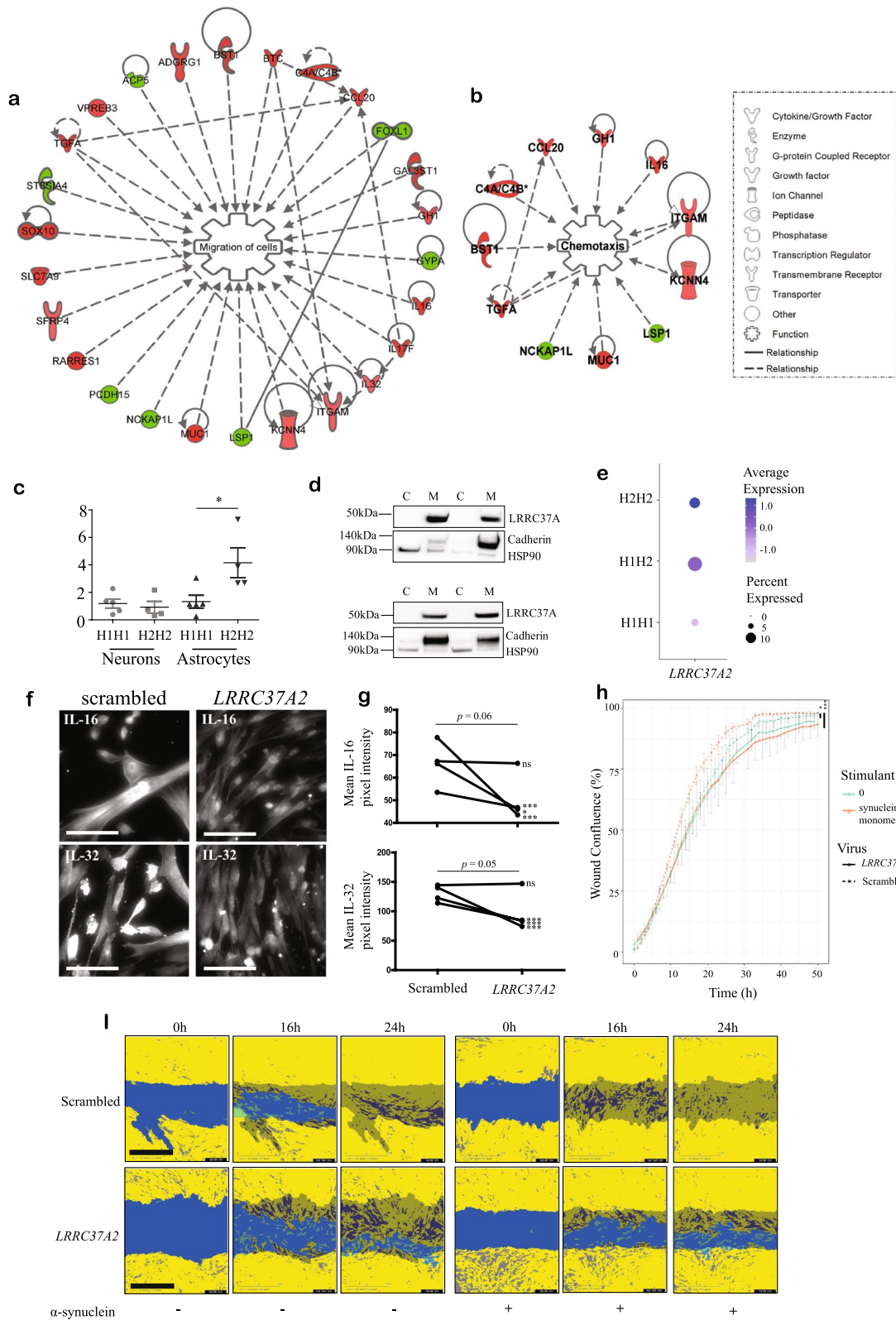


Fig. 3 (See legend on previous page.)

astrocytes, but not in H2 neuronal cultures (Fig. 3C, Figure S6H), suggesting that H1/H2-associated *LRRC37A/2* expression changes may be specifically impacting astroglial gene expression and function. We also confirmed that *LRRC37A/2* was present in the plasma membrane in both iPSC-derived neurons and astrocytes by isolating cytosolic and membrane-associated proteins from each cell type and analyzing the resulting fractions by western blot (Fig. 3D). We further confirmed that 17q21.31 haplotype may be more relevant to astrocyte function by comparing *LRRC37A/2* expression in single nuclei sequencing data (snuc-seq) from human prefrontal cortex [33] (Figure S6I). We found that *LRRC37A2* was more highly expressed in all cell types compared to *LRRC37A*, indicating that this may be the driver behind any functional differences due to haplotype (Figure S6J). Furthermore, there was a clear H2 dose-dependent effect on the proportion of *LRRC37A2*-expressing astrocytes and level of expression (Fig. 3E) although due to the small population of astrocytes in this dataset (Figure S6I), the difference in *LRRC37A2* expression between H1H1 and H2H2 astrocytes did not pass multiple test correction. In contrast, while there were fewer *LRRC37A2*-expressing cells in H1H1 cells compared to H1H2 and H2H2, there was no dose-dependent effect of the H2 haplotype on *LRRC37A2* expression in either excitatory or inhibitory neuronal populations (Figure S6K).

To further validate the function of *LRRC37A2* expression in astrocytes, we knocked down its expression in iPSC-derived astrocytes using lentiviral *LRRC37A2* shRNA, which was confirmed by qRT-PCR (Figure S7A). We then confirmed that genes that were upregulated in HEK293T cells in response to *LRRC37A2* overexpression were reduced in astrocytes following *LRRC37A2* knock-down (Figure S7A), thus validating the relevance of our HEK293T gene expression data. In addition, consistent with the RNA-seq data, we then demonstrated significantly reduced expression of cytokines IL-32 and IL-16 in *LRRC37A2* knock-down astrocytes by immunofluorescence in 3/4 donor lines examined (Fig. 3F-G, Figure S7B-C). In order to determine whether *LRRC37A2* expression was involved in cellular migration and response to stimulants, we conducted a scratch wound repair assay in the presence or absence of monomeric α -synuclein and measured the rate of wound repair over the course of 50 h (Fig. 3H-I). In the absence of α -synuclein, there was no significant difference in the rate of wound repair (% wound confluence) over time between *LRRC37A2* shRNA and scrambled control groups ($p > 0.05$). Treatment with monomeric α -synuclein increased the rate of wound repair in scrambled control astrocytes ($p = 0.05$) indicating a responsiveness to α -synuclein as a stimulant. However, *LRRC37A2* knock down astrocytes

demonstrated no such response to α -synuclein exposure, and their rate of wound repair was significantly slower than compared to controls treated with α -synuclein ($p < 0.001$) (Fig. 3H-I). These data confirm a likely role for *LRRC37A2* expression in disease-relevant astrocytic functions including inflammation, cellular migration and responsiveness to α -synuclein.

LRRC37A2 interacts with soluble and aggregated α -synuclein in human substantia nigra.

In order to assess whether *LRRC37A/2* was expressed in mature astrocytes in human brain tissue, we carried out multiplex immunofluorescence staining in human substantia nigra from PD, PSP and aged controls (Fig. 4A). We found that in all cases, *LRRC37A/2* co-localized with the astrocyte marker GFAP, but not the microglia marker IBA1 (Fig. 4A, Figure S7D). In contrast, α -synuclein positivity was observed only in PD substantia nigra, and hyperphosphorylated tau (labeled with AT8) was present only in PSP brain (Fig. 4A). Interestingly, in regions with Lewy body pathology there was reduced staining intensity of *LRRC37A/2* in astrocytes, and colocalization of *LRRC37A/2* with Lewy bodies (Fig. 4A). However, there was no association between tau AT8 positivity and *LRRC37A/2* expression in PSP substantia nigra (Fig. 4A), indicating that *LRRC37A/2* accumulation is specific to PD pathology. To validate the association of *LRRC37A/2* with α -synuclein, we performed co-immunoprecipitation from control, PSP and PD substantia nigra tissue (Fig. 4B). We found that soluble α -synuclein bound *LRRC37A/2* in all cases, whereas IgG alone did not (Fig. 4B), indicating that *LRRC37A/2* and α -synuclein likely form a complex in human brain that becomes disordered in the context of PD pathogenesis. Furthermore, analysis of publicly available snuc-seq data from PD and control midbrain [34] indicated a trend towards reduced *LRRC37A2* expression in PD astrocytes compared to controls (Figure S7E-F), consistent with a potentially protective effect of increased *LRRC37A/2* expression. These data are not only the first to identify a role for *LRRC37A/2* in astrocytes, but are the first to link the genetic association at the 17q21.31 locus with PD pathology.

Discussion

By constructing discrete sub-haplotype blocks across the 17q21.31 H1 locus, we have identified multiple novel H1 sub-haplotypes associated with variable levels of PD risk, independent of the previously constructed sub-haplotypes across *MAPT* [30]. The association of some of these blocks with PD risk was inconsistent between stage 1 and stage 2 analyses, possibly due to genotyping and imputation error. We were able to identify blocks and

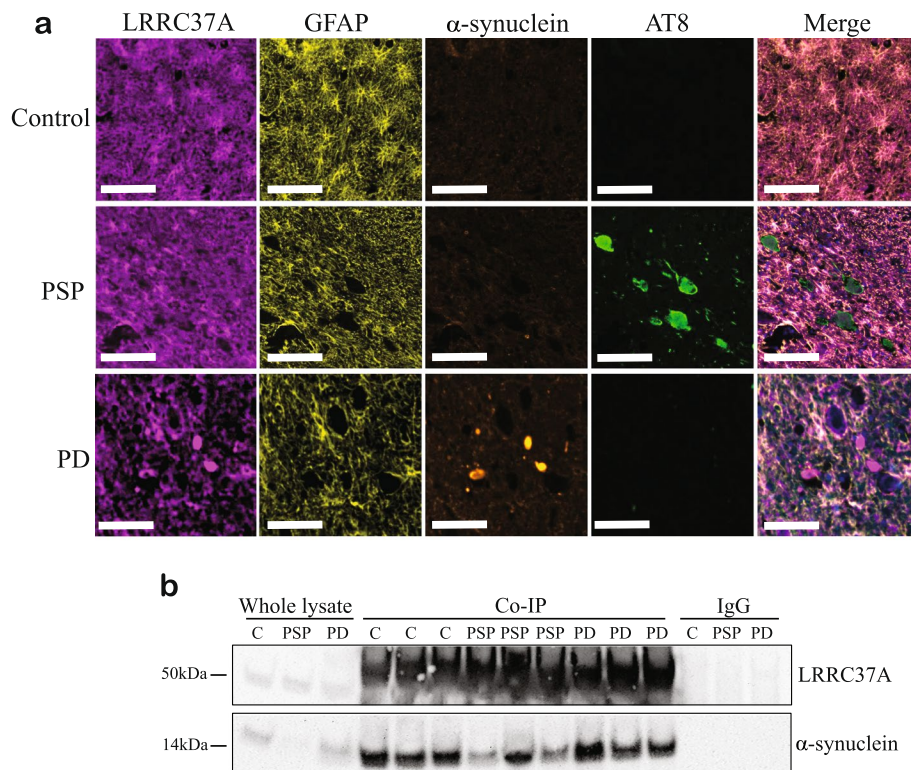


Fig. 4 LRRC37A/2 is expressed in astrocytes in the substantia nigra and is co-localized with α -synuclein **A**. Representative images from multiplex immunofluorescent staining of human control, PSP and PD substantia nigra sections with astrocyte marker GFAP, LRRC37A, α -synuclein and pathologically phosphorylated Tau (AT8). Scale bar = 100 μ m, $N=4-5$. **B**. Co-immunoprecipitation (Co-IP) of LRRC37A (top panel) with soluble α -synuclein (bottom panel) in substantia nigra from control (C), PSP and PD brain, $N=3$. Whole protein lysates and IgG only controls were included for comparison

sub-haplotypes with common protective effects across populations. The *MAPT* gene, encoding the microtubule associated protein tau, is central to this locus and is likely the causal gene for other neurodegenerative disorders genetically associated with the H1 haplotype, such as PSP and CBD [2, 3], given that they are characterized neuropathologically by tau hyperphosphorylation and accumulation. Recently, reduced expression of *MAPT-AS1* has been identified in PD substantia nigra [38] and has been shown to have an inverse correlation with *MAPT* expression [39], suggesting a potential role for *MAPT* expression in PD pathogenesis. However, we did not observe any association between *MAPT* expression or splicing and 17q21.31 haplotype or sub-haplotypes in our analyses, indicating that any disease-associated *MAPT* regulation in PD brain may not be due to haplotype. Furthermore, while tau pathology can occur alongside α -synuclein inclusions in the substantia nigra [16, 17], it is not a typical neuropathological feature of PD [15]. The causal gene underlying the genetic association across the 17q21.31 locus with PD risk has therefore been unclear, although a recent study proposed that H1-associated

variants in *KANSL1* alter mitophagy [40]. In contrast, we did not find any effect of our PD-associated H1 sub-haplotypes on either *KANSL1* expression or copy number, but did observe a consistent association with the expression of another gene in the locus, *LRRC37A/2*. However, these data do not rule out that *KANSL1* variants may alter disease risk independently of *LRRC37A/2* expression between the major haplotype clades and H1 sub-haplotypes.

We found that protective H1 sub-haplotypes were associated with increased expression of *LRRC37A/2*. This is consistent with increased expression of these genes in the protective H2 haplotype, suggesting that there is likely a shared mechanism of protection from PD between H2 and specific sub-haplotypes of H1. Furthermore, analysis of CNVs in the 3' distal end of the 17q21.31 locus suggested that protective sub-haplotypes were tagging structural variants defined by increased gamma region [20] and *LRRC37A/2* copy number, which likely underlies the increased expression of these genes. *LRRC37A* is a core duplcon on chromosome 17 [41] and is present at the inversion breakpoint of the 17q21.31

locus; it has been hypothesized that its propensity for CNVs is responsible for the evolutionary toggling of this region that resulted in the distinct H1 and H2 haplotypes [42]. Due to the complex structural variation surrounding *LRRC37A* and the presence of its paralog *LRRC37A2*, it is challenging to genotype or sequence this region of the genome. As such, our analyses have not been able to separate the contribution of each gene and have considered them together, however *LRRC37A2* expression was consistently higher in both neurons and glial cells than *LRRC37A* and may therefore be the most relevant gene. As a consequence of the CNVs in this region, genotyping data across *LRRC37A* and *LRRC37A2* is of low confidence and quality, and as such is excluded from GWAS analyses, as is visible in any association plot, and likely explains why the peak genetic signal for PD association was close to *MAPT* and *KANSL1*. The association between *LRRC37A/2* variants and any disease or phenotype has therefore never been tested, and it is likely that additional variation within *LRRC37A/2* itself is contributing to its altered expression and function that may also impact PD risk. Little is known about the function of *LRRC37A/2*, although it has been associated with an increased immune and inflammatory response [43], as well as with cellular migration and synapse formation [41]. Despite conducting our RNA-seq analysis of *LRRC37A/2* overexpression in HEK293T cells, we observe enrichment of pathways consistent with these data; we found that increased *LRRC37A/2* expression upregulated cellular migration and chemotaxis pathways, which are both essential mechanisms involved in wound healing and inflammation. Furthermore, we validated these gene expression changes and demonstrated a role for *LRRC37A2* in astroglial migration in iPSC-derived astrocytes.

Within these pathways we observe increased expression of pro-inflammatory cytokines *IL17* and *IL32*, as well as the chemoattractant *IL16*, each of which are involved in the astrocytic inflammatory response [31, 32]. Neuroinflammation of the substantia nigra is considered a characteristic feature of PD in addition to neuronal loss [44, 45], and many genes associated with PD, such as *GBA*, *LRRK2* and *PINK1* are thought to have a role in the inflammatory response in astrocytes [24, 46]. Furthermore, the most significantly enriched pathway in our analysis, *Neuroactive-ligand receptor interaction*, is also involved in the inflammatory response and has previously been associated with PD; this pathway was significantly enriched in a functional assessment of PD GWAS signals [47], and is targeted by microRNAs that are upregulated in a *Drosophila* model of PD [48]. We also observe upregulation of *TGFA*, the infusion of which into the forebrain of a rat model of PD increased the

proliferation of neuronal and glial progenitors and the production of dopaminergic neurons to the substantia nigra [49], indicating that this may be a protective growth factor against neuronal loss in PD. *LRRC37A/2* overexpression in HEK293T cells was therefore able to recapitulate pathways associated with PD, despite being a cell type with limited relevance to PD pathogenesis.

As these expression data were indicative of pathways relevant to astrocyte biology, and we found that *LRRC37A/2*-associated gene expression changes were apparent in astrocytes but not neurons, we hypothesized that this was likely the most relevant cell type for *LRRC37A/2* expression. Indeed, in human substantia nigra tissue we observe localization of *LRRC37A/2* specifically in astrocytes. The contribution of astrocytic dysfunction to PD pathogenesis has gained attention in recent years, and is hypothesized to be a causal mechanism for the initiation and progression of PD [22–25]. Many genes associated with PD risk are expressed in astrocytes, the functions of which converge on the inflammatory response, lipid handling, mitochondrial health and lysosomal function [24]. Our finding that *LRRC37A/2* is expressed in astrocytes and plays a role in the inflammatory response is therefore consistent with known pathogenic mechanisms of PD. Furthermore, we demonstrate that *LRRC37A2* expression may play a role in the detection of extracellular monomeric α -synuclein by astrocytes, and consequently impacts migration and tissue repair. α -synuclein has previously been identified as a stimulant for astrocytes [50], inducing a reactive state [51]. This mechanism was impaired in the context of reduced *LRRC37A2* expression, indicating that appropriate detection and response to stimulants by astrocytes is likely a protective mechanism against neuronal death.

However, the role of astroglial inflammation in PD is unclear [22]. As a further complication, in vitro studies of human astrocyte cultures indicate that α -synuclein induces the release of pro-inflammatory cytokines [22, 25], but these cells also release protective molecules such as GDNF in response to dopaminergic neuronal damage, and such trophic support may benefit neuronal survival [22]. In addition, the substantia nigra is considered to be particularly susceptible in PD as dopaminergic neurons in this region are surrounded by the lowest proportion of astrocytes in the brain [52]. Whether an inflammatory response in this context would be protective or exacerbate neuronal death is therefore unknown. As our data suggest increased *LRRC37A/2* expression is protective and associated with increased expression of pro-inflammatory cytokines, astroglial inflammation in response to α -synuclein may therefore be protective.

Interestingly, we observe an interaction between *LRRC37A/2* and soluble α -synuclein, as well as

co-localization of LRR37A/2 with Lewy bodies in PD substantia nigra. The function and mechanism of this interaction is untested, although it is likely that a complex is formed in astrocytes and propagated to neurons. iPSC-astrocytes have been reported as expressing low levels of endogenous α -synuclein, which is increased in cells derived from PD patients [25], and α -synuclein released from neuronal axon terminals is taken up by astrocytes [28], which can be further transferred to neurons [23, 29]. This raises the possibility that LRR37A/2 may influence α -synuclein release, aggregation and/or propagation.

Conclusions

In conclusion, we have identified novel sub-haplotype variants of the 17q21.31 H1 clade significantly associated with protection against PD. While the genetic association across this locus is typically ascribed to *MAPT* or *KANSL1*, we find evidence for the involvement of a novel gene, *LRR37A/2*, in PD risk. We propose that in a similar mechanism to other PD-associated genes, *LRR37A/2* is expressed in astrocytes and plays a role in the regulation of astroglial inflammation, specifically in the release of pro-inflammatory cytokines, chemotaxis and cellular migration. Importantly, we demonstrate that *LRR37A/2* interacts and co-localizes with α -synuclein and Lewy bodies, thus indicating a potential modifying role in the formation of PD pathology. These findings link the genetic association at the 17q21.31 H1 locus with PD pathology, and support the hypothesis of astroglial dysfunction as a key contributing factor to PD disease pathogenesis.

Methods

Genotype data treatment

Case and control data from several cohorts from the International Parkinson's Disease Genetics Consortium (IPDGC; NIA, GER, FIN, NL, SP, McGill) [6, 9, 10] was kindly shared by Drs. Nalls, Singleton and Bandres-Ciga (NIH, Bethesda, MD; Tables S2, S6).

Pre-imputation QC

Each dataset was obtained with different QC filters already applied, and so were all subsequently passed through the same, more stringent QC pipeline to ensure consistency. Plink v1.9 [53] was used to perform quality control for all datasets. First, SNPs were filtered by a 98% call rate, and remaining SNPs with a MAF < 1% were excluded. Individuals with < 98% genotyping rate were then removed. To determine and correct for population stratification, principal components analysis was carried out in combination with Hapmap YRI, CEU and CHB populations [54] using EIGENSOFT [55]. Samples that did not cluster with the CEU European ancestry

population were excluded. Identity by descent analysis was then conducted, and related individuals or potential sample duplicates ($Z_0 \leq 0.8$) were removed. We were unable to assess discordant sex information on data acquired from other sources, as the required information for this analysis was not provided to us. Variants that deviated from Hardy Weinberg equilibrium at a significance threshold $< 1 \times 10^{-4}$ were then removed. Chromosome 17 was then isolated and screened for strand mismatches.

Imputation and post-imputation QC

Filtered chromosome 17 data from each cohort was submitted individually to the Michigan imputation server [56] (<https://imputationserver.sph.umich.edu>) and imputed against the HRC r1.1 2016 panel using Eagle v2.3 phasing. Following imputation, SNPs with an $r^2 < 0.3$ were removed, and remaining SNPs were filtered for a 99% call rate. Genotyping call rates for individuals were again filtered at 99%, and SNPs that deviated from Hardy–Weinberg equilibrium at a significance threshold $< 1 \times 10^{-6}$ were excluded. Individual cohorts were then merged, and finally filtered once more with a SNP call rate of 99%. Prior to analysis, variants were filtered to exclude SNPs with a MAF < 0.01.

Single SNP association analyses

Logistic regression association analyses using an additive model were carried out in SNP and Variation Suite v8.8.1 (SVS8) software (Golden Helix, Inc., Bozeman, MT, www.goldenhelix.com). As all potential covariate information was not available, the model was corrected using the first 10 principal components as calculated by SVS8. Associations were initially carried out on the entire cohort in order to confirm the 17q21.31 H1/H2 haplotype association. The data was then filtered for H1 homozygotes only, using tag SNP rs8070723 and the association analysis was repeated with the same parameters.

Meta-analysis of SNP effects across multiple datasets was carried out using the R package rmeta [57] using both Random Effects (DerSimonian-Laird) and Fixed Effects (Mantel–Haenszel) approaches. Calculation and visualization of linkage disequilibrium (LD) over large genomic ranges was carried out in SVS8 using both r^2 and D' . Inspection of LD between individual SNPs of interest was carried out using Haploview [58].

Haplotype block construction and association

Haplotype blocks were constructed in SVS8 using the D' measure of LD. Blocks were defined using guidelines as described by Gabriel et al. (2002) [59]. Each block contained a maximum of 15 markers within 160 kb of each other, with a D' upper confidence bound ≥ 0.98 and a

lower confidence bound ≥ 0.7 . Haplotypes were estimated using an expectation–maximization (EM) algorithm with 50 iterations, and a convergence tolerance of 0.0001. Sub-haplotypes with a frequency < 0.01 were excluded from further analysis. Case–control association analyses were carried out per block using a logistic regression model. Odds ratios and associated Fisher’s exact p-values were calculated for each sub-haplotype within each block using the R package *epitools* [60].

MAPT sub-haplotypes were defined as previously described [30, 61]. Sub-haplotypes were estimated for each individual in Stage 1 data as described above, and case–control association analysis was conducted for association with each sub-haplotype as described above.

WGS data

A subset of processed whole genome sequencing data was obtained from the AMP-PD Parkinson’s Progression Markers Initiative (PPMI) (amp-pd.org/unified-cohorts/ppmi). Data were further processed using a publicly available, in-house WGS QC pipeline (<https://github.com/ricardovialle/WGS-QC-Pipeline>). Briefly, data were filtered to exclude variants with MAF $< 1\%$, missingness $> 5\%$, read depth $< 200,000$, mapping quality < 58.75 and > 61.25 , and with an inbreeding coefficient < -0.8 . Samples were excluded with a missingness $> 10\%$ and relatedness threshold > 0.125 . This resulted in a final dataset of 3074 individuals. Sub-haplotypes were phased and estimated as described above, and frequencies for each H1.1, H1.2 and H1.3 sub-haplotype were determined.

Human brain expression analysis

Publicly available RNA-seq expression data from human postmortem dorsolateral prefrontal (PFC) and temporal (TCX) cortices (Table S5) and associated genotype data were obtained from Synapse (synapse.org; The Religious Orders Study and Memory and Aging Project (ROSMAP) syn3219045; MayoRNAseq syn5550404; CommonMind Consortium syn2759792). Genotype data for chromosome 17 underwent the same QC and imputation pipeline as described above. Data were stratified by 17q21.31 H1/H2 haplotype using the H2 tag SNP rs8070723. For sub-haplotype analysis, blocks previously defined in the PD analysis were applied to the genotype data and haplotypes were estimated in the same manner. Statistical analysis was carried out in R version 3.4.0. For analysis of *MAPT* splicing, percent spliced in (PSI) values were generated for exons 2, 3 and 10 using Mixture of Isoforms (MISO) [62]. Gene expression and PSI residuals were generated by linear regression using sex, age of death, post-mortem interval and RNA integrity score as

covariates. The resulting residuals were then transformed into z-scores and combined across datasets. Statistical differences in gene expression between genotypes and sub-haplotypes were determined by linear regression applied to the adjusted and combined z-scores.

dPCR

Human genomic DNA and accompanying genotype data was kindly provided by Drs. Raj, Cray and Charney (Mount Sinai School of Medicine, NY) and by the Alzheimer’s Disease Research Center (ADRC; Table S5). Sub-haplotypes were called from these genotype data in the same manner as described above. To examine copy number variation in the 17q21.31 locus, digital PCR was carried out using the ThermoFisher QuantStudio 3D digital PCR chip system. Taqman dPCR probes for loci within the alpha, beta and gamma CNV regions [20], as well as within *LRRC37A* and *MAPT* were selected for analysis (Table S7).

Cell lines

Human induced pluripotent stem cells (iPSCs) were obtained from the Knight Alzheimer’s Disease Research Center at Washington University [63], the NIH Childhood-onset Schizophrenia study [64], the New York Stem Cell Foundation (NYSCF) and the New South Wales Brain Bank (NSWBB) (Table S8). The Icahn School of Medicine at Mount Sinai IRB reviewed the relevant operating protocols as well as this specific study and determined it was exempt from approval.

Cell culture

Unless otherwise specified, all cell culture materials were obtained from ThermoFisher Scientific. Human embryonic kidney cells (HEK293T) were cultured in Dulbecco’s Modified Eagle Medium/F-12 with HEPES, supplemented with 10% fetal bovine serum (FBS) and 1% Penicillin–Streptomycin. Cells were passaged every 3–4 days using Trypsin–EDTA (0.25%). For *LRRC37A/2* overexpression experiments, HEK293T cells were seeded at a density of 1.4×10^5 cells per well in 6-well plates and transfected with 0.5–2.5 μg of *LRRC37A* plasmid (Origene) or empty vector control (Origene) using Lipofectamine 3000. Cells were harvested 48 h after transfection.

For qRT-PCR, protein biochemistry and *LRRC37A/2* knockdown experiments, iPSC lines (Table S8) were maintained in complete StemFlex media supplemented with 1% penicillin/streptomycin on Matrigel (BD biosciences), and were differentiated to neural progenitor cells (NPCs) as previously described [65]. Forebrain

neuron-enriched cultures and astrocyte cultures were differentiated from NPCs as previously described [65, 66]. Neuronal and astrocytic identity was confirmed by immunofluorescence for common neuronal and astrocytic markers (MAP2 (Abcam), Tuj1 (Cell Signaling Technologies), S100 β (Sigma Aldrich) and EAAT1 (Abcam)).

Genomic DNA was extracted using the DNeasy Blood and Tissue kit (Qiagen) and underwent genotyping with Taqman assays for H2 tag SNPs rs8070723 and rs1052553 in order to confirm 17q21.31 haplotype.

LRRC37A2 knockdown

iPSC-derived astrocytes from four donors were seeded at low density in a 24-well plate, and were infected with either *LRRC37A2* shRNA viral particles (Santa Cruz) or scrambled control viral particles (Origene) with an MOI = 10 for 24 h. Infected cells were then washed with fresh media, then maintained and expanded as previously described [67]. *LRRC37A2* knockdown was confirmed by qRT-PCR using commercially available Taqman probes, and was normalized to *GAPDH* expression.

Scratch wound assay

LRRC37A2 and scrambled control shRNA-treated astrocytes were seeded at high density into IncuCyte ImageLock plates coated with Matrigel (Corning). Upon reaching confluency, scratch wounds were applied to each well using the Incucyte WoundMaker tool, and cell culture media was replaced in order to remove dead cells and debris. Astrocytes were then either treated with 200 ng/ml monomeric recombinant α -synuclein (Abcam) or the equivalent volume of PBS. Cells were then imaged every hour for 50 h in the IncuCyte live cell imaging platform. Images were analyzed using the IncuCyte software with Scratch Wound module for automated detection of wound confluency and cell density.

Immunofluorescence and image analysis

iPSC-derived astrocytes were grown in 96-well plates and fixed with 10% Formalin (Sigma Aldrich) for 15 min at room temperature, followed by 3 \times washes with PBS. Fixed cells were permeabilized with 0.1% Triton x-100 and blocked with 1% BSA in PBS for 30 min at room temperature. Cells were incubated with antibodies against either IL-16 or IL-32 (both Abcam) overnight at 4 $^{\circ}$ C, washed \times 3 with PBS and incubated with secondary antibodies (AlexaFluor anti-rabbit 647, ThermoFisher Scientific) at 1:100 for 2 h at room temperature. Cells were counterstained with DAPI for 10 min at room temperature, then washed \times 3 with PBS. Labeled astrocytes underwent automated imaging on the ThermoFisher CellInsight CX7 High Content Screening platform with a

40 \times objective and widefield imaging. Exposure times for IL-16 and IL-32 were manually fixed across all fields and wells. Sixteen images per cell line were arbitrarily taken per condition. Image intensity analysis was carried out using ImageJ v1.53 s. A minimum grey intensity threshold was set to enable cell detection by positive pixels, and mean grey intensity was determined across positive pixels per field of view. qRT-PCR.

RNA was extracted from HEK293T cells, iPSC-derived neurons, astrocytes and human brain tissue using the RNeasy Mini kit (Qiagen) and reverse transcribed using the High-Capacity RNA-to-cDNA kit (ThermoFisher Scientific). Gene expression was measured by commercially available Taqman qRT-PCR assays.

RNA-seq

RNA was prepared as described above. Library preparation with poly-A selection and sequencing with 150 base pair paired-end reads was carried out at Genewiz. Sequenced reads were trimmed for Illumina TruSeq adapters, and quantified for gene expression values in TPM (Transcripts Per Kilobase Million) using Salmon [68] guided by the GENCODE human transcriptome model (GRCh38 version 28, Ensembl 92). TPM data was imported into the R (version 3.5.1) programming environment for visualization and analysis, and differential expression of *LRRC37A/2* overexpression compared to the control was analyzed using the moderated t-test implemented in limma [69]. Differentially expressed genes (DEGs) were defined by $\pm \geq 1.5$ expression fold change and adjusted $p < 0.05$. Gene set enrichment analysis was performed with the Broad Institute's MSigDB annotations [70]. Analysis of GO enrichment terms was carried out using g:Profiler (<https://biit.cs.ut.ee/gprofiler/gost>) [71, 72] and visualized using Cytoscape v3.7.1 [73] with the EnrichmentMap [74] plugin. Additional pathway analyses were carried out using Ingenuity Pathway Analysis (QIAGEN Inc., <https://www.qiagenbioinformatics.com/products/ingenuitypathway-analysis>) using genes with a fold change $\pm \geq 1$.

Protein biochemistry

Membrane and cytosolic proteins were isolated from HEK293T cells, iPSC-derived neurons and iPSC-derived astrocytes using the MEM-PER Plus Membrane Protein Extraction Kit (ThermoFisher Scientific), and protein concentrations were determined by bicinchoninic acid (BCA) assay (ThermoFisher Scientific). For western blotting, protein fractions were subject to SDS-PAGE electrophoresis through BOLT Bis-Tris gels (ThermoFisher Scientific) and were blotted onto nitrocellulose membranes. Membrane fractions were confirmed by labeling with an anti-pan-Cadherin antibody (Cell Signaling

Technology), and cytosolic fractions were confirmed by labelling with anti-HSP90 (Cell Signaling Technology). Membranes were stripped using Restore plus western blot stripping buffer and re-probed with an anti-LRR37A antibody (ThermoFisher Scientific).

Single nuclei sequencing data analysis

PD midbrain snuc-seq gene counts and cell metadata³⁴ were downloaded from GEO (GSE157783). AD PFC snuc-seq filtered gene counts and cell metadata³³ were downloaded from Synapse (syn18681734). Data underwent filtering and processing using Seurat v4.075,76. Briefly, for PD midbrain data, cells expressing fewer than 200 genes, with fewer than 2500 reads and with greater than 10% mitochondrial gene expression were removed. Count data was normalized using SCTransform⁷⁷, while regressing out mitochondrial rate, number of expressed genes and the number of reads per cell. Principal components analysis was carried out using the top 3000 most variable genes, and data reduction was performed with UMAP⁷⁸. Cell types were determined using the provided annotations on GEO. Astrocytes were then isolated and re-scaled. Differential gene expression between PD and control cells was carried out on the raw count data using the MAST model with percent mitochondrial gene expression as a covariate. For AD PFC data, cells with fewer than 2000 reads, expressing fewer than 200 genes and abnormally high ratios of counts mapped to mitochondrial genes relative to the total number of detected genes were removed. Count data was normalized using the SCANPY package⁷⁹ and principal components analysis and data reduction was carried out as described above. Cell types were determined using the annotations provided in the cell metadata, and genotypes were determined using genotype data from the ROSMAP cohort as described above. Differential gene expression between haplotypes was carried out on the raw count data using the MAST model with pathological diagnosis, sex and age at death as covariates.

OPAL multiplex labelling

Formalin fixed paraffin embedded substantia nigra sections from human controls ($N=4$), PSP ($N=5$) and PD ($N=5$) cases were acquired from the Mount Sinai Neuropathology Brain Bank, with neuropathological diagnosis being determined by Dr. John Crary. All post-mortem tissues were collected in accordance with the relevant guidelines and regulations at the Icahn School of Medicine at Mount Sinai. Multiplexed immunofluorescent staining was carried out on 4–6 μm sections using the Opal Polaris 7 color IHC detection kit (Akoya biosciences) according to manufacturer's instructions. Briefly, slides were baked for 1 h at 65 °C, then deparaffinized with xylene

and rehydrated with a graded series of ethanol concentrations. For epitope retrieval, slides were microwaved in AR buffer for 45 s at 100% power, followed by an additional 15 min at 20% power. After cooling, slides were blocked for 10 min in blocking buffer then incubated with the first primary antibody at room temperature for 30 min. Slides were rinsed three times in TBS-T, then incubated with the secondary polymer HRP for 1 h at room temperature. After additional washes, the first Opal fluorophore was incubated with the slides for 10 min at room temperature, followed by further washes in TBS-T. This process was repeated from the microwave treatment step for each additional primary antibody, followed by one final repetition of the microwave treatment to strip the primary-secondary antibody complex from the tissue. Once all primary antibodies had been introduced, slides were counterstained with DAPI for 5 min at room temperature, washed with TBS-T and coverslips were mounted using ProLong Diamond Antifade mounting reagent (ThermoFisher Scientific). Multispectral imaging was carried out using the Vectra Quantitative Pathology Imaging system, applying quantitative unmixing of fluorophores and removal of tissue autofluorescence. Images were visualized using the HALO image analysis platform (Indica Labs).

Co-Immunoprecipitation

Frozen substantia nigra tissue was selected from the same Control ($N=3$), PSP ($N=3$) and PD ($N=3$) cases used for OPAL multiplex immunofluorescence. Protein lysates were generated using cell lysis buffer (NEB) and brief sonication on ice, followed by centrifugation to pellet insoluble material. Co-immunoprecipitation was carried out using the Dynabeads Protein G immunoprecipitation kit (ThermoFisher Scientific), with an anti- α -synuclein antibody (Abcam) as bait. Proteins bound to beads were eluted and assayed by western blot (as described above) and probed with an anti-LRR37A antibody (ThermoFisher Scientific). Whole protein lysate and IgG only controls were run on the same blots.

Abbreviations

PD: Parkinson's disease; AD: Alzheimer's disease; CBD: Corticobasal degeneration; PSP: Progressive supranuclear palsy; dPCR: Digital polymerase chain reaction; qRT-PCR: Quantitative reverse transcription polymerase chain reaction; DNA: Deoxyribonucleic acid; RNA-seq: Ribonucleic acid sequencing; LD: Linkage disequilibrium; Mb: Megabase; OR: Odds ratio; SNP: Single nucleotide polymorphism; CI: Confidence interval; CNV: Copy number variation; GO: Gene ontology; IPA: Ingenuity pathway analysis; iPSC: Induced pluripotent stem cell; GWAS: Genome-wide association study; IgG: Immunoglobulin G; AMP-AD: Accelerating Medicines Partnership Alzheimer's disease; PFC: Prefrontal cortex; TCX: Temporal cortex; MAPT: Microtubule associated protein tau; LRR37A/2: Leucine rich repeat containing 37A and 37A2; KANSL1: KAT8 regulatory NSL complex subunit 1; IL17F: Interleukin 17F; IL32: Interleukin 32; IL16: Interleukin 16; CD4: Cluster of differentiation 4; GFAP: Glial fibrillary acidic protein; IBA1: Ionized calcium binding adaptor molecule 1; GBA: Glucosylceramidase beta;

LRRK2: Leucine rich repeat kinase 2; PINK1: PTEN induced kinase 1; TGFA: Transforming growth factor alpha; GDNF: Glial cell line-derived neurotrophic factor; IPDGC: International parkinson's disease genetics consortium; NIA: National institute of aging; GER: German; FIN: Finnish; NL: Netherlands; SP: Spanish; QC: Quality control; MAF: Minor allele frequency; YRI: Yoruba; CEU: Northern Europeans from Utah; CHB: Han Chinese in Beijing; HRC: Haplotype reference consortium; SVS: SNP variation suite; EM: Expectation-maximization; PSI: Percent spliced in; MISO: Mixture of isoforms; ADRC: Alzheimer's disease research center; IRB: Institutional review board; FBS: Fetal bovine serum; NPC: Neural progenitor cell; TPM: Transcripts per million; DEG: Differentially expressed gene; BCA: Bicinchoninic acid; SDS-PAGE: Sodium dodecyl sulfate polyacrylamide gel electrophoresis; IHC: Immunohistochemistry; AR: Antigen retrieval; HRP: Horseradish peroxidase; TBS-T: Tris-buffered saline with tween.

Supplementary Information

The online version contains supplementary material available at <https://doi.org/10.1186/s13024-022-00551-x>.

- Additional file 1.** Supplementary fig 1
- Additional file 2.** Supplementary fig 2
- Additional file 3.** Supplementary fig 3
- Additional file 4.** Supplementary fig 4
- Additional file 5.** Supplementary fig 5
- Additional file 6.** Supplementary fig 6
- Additional file 7.** Supplementary fig 7
- Additional file 8.** Supplementary table 1
- Additional file 9.** Supplementary table 2
- Additional file 10.** Supplementary table 3
- Additional file 11.** Supplementary table 4
- Additional file 12.** Supplementary table 5
- Additional file 13.** Supplementary table 6
- Additional file 14.** Supplementary table 7
- Additional file 15.** Supplementary table 8

Acknowledgements

We thank the Icahn School of Medicine at Mount Sinai Neuropathology Brain Bank CoRE for supplying post-mortem human brain tissues for analysis. We are grateful to the bank bank participants and their families for their contributions to research. Data used in the preparation of this article were obtained from the Accelerating Medicine Partnership[®] (AMP[®]) Parkinson's Disease (AMP PD) Knowledge Platform. For up-to-date information on the study, visit <https://www.amp-pd.org>. The AMP[®] PD program is a public-private partnership managed by the Foundation for the National Institutes of Health and funded by the National Institute of Neurological Disorders and Stroke (NINDS) in partnership with the Aligning Science Across Parkinson's (ASAP) initiative; Celgene Corporation, a subsidiary of Bristol-Myers Squibb Company; Glaxo-SmithKline plc (GSK); The Michael J. Fox Foundation for Parkinson's Research; Pfizer Inc.; Sanofi US Services Inc.; and Verily Life Sciences. ACCELERATING MEDICINES PARTNERSHIP and AMP are registered service marks of the U.S. Department of Health and Human Services. Genome sequence data for the Lewy body dementia case-control cohort were generated at the Intramural Research Program of the U.S. National Institutes of Health. The study was supported in part by the National Institute on Aging (program #: 1ZIAAG000935) and the National Institute of Neurological Disorders and Stroke (program #: 1ZIAN0003154). PPMI is sponsored by The Michael J. Fox Foundation for Parkinson's Research and supported by a consortium of scientific partners: [list the full names of all of the PPMI funding partners found at <https://www.ppmi-info.org/about-ppmi/who-we-are/study-sponsors>]. The PPMI investigators have not participated in reviewing the data analysis or content of the manuscript. For up-to-date information on the study, visit www.ppmi-info.org. We are grateful to the New York Stem Cell Foundation for contributing iPSC lines for this study, as well as the New South Wales Brain Bank. Peripheral blood

mononuclear cells (PBMCs) were obtained from the New South Wales Brain Bank at Neuroscience Research Australia, which is supported by the University of New South Wales and Neuroscience Research Australia. We thank the Icahn School of Medicine at Mount Sinai core for iPSC reprogramming services.

Author contributions

Conceptualization: KRB, JFC, AMG. **Methodology:** KRB, JDC. **Validation:** KRB, DAP. **Formal Analysis:** KRB, DAP, YL, SB-C, ZG-O, PH, AS, SB, TP. **Investigation:** KRB, DAP, YL. **Resources:** AC, CMK, SJF, BHK, IP, YJP, AC, TR, JFC, AMG. **Data Curation:** KRB, YL, SB-C, ZG-O, PH, AS, SB, IPDGC, TP. **Writing – Original Draft:** KRB. **Writing – Review and Editing:** KRB, YL, AER, SB-C, ZG-O, CMK, IP, TP, TR, JFC, AMG. **Visualization:** KRB, TP. **Supervision:** AMG. **Funding Acquisition:** KRB, JFC, AMG. All authors read and approved the final manuscript.

Funding

This work was supported by funding from the BrightFocus Foundation (KRB), Association for Frontotemporal Degeneration (KRB) and CurePSP (KRB). The recruitment and clinical characterization of research participants at Washington University were supported by NIH P50 AG05681, P01 AG03991, and P01 AG026276. NIH AG062683 (J.TCW), Rainwater Charitable Organization (CMK), NIH AG046374 (CMK). The McGill cohort was supported by grants from the Michael J. Fox Foundation, the Canadian Consortium on Neurodegeneration in Aging (CCNA), the Canada First Research Excellence Fund (CFREF), awarded to McGill University for the Healthy Brains for Healthy Lives (HBHL) program, and Parkinson Canada. ZGO is supported by the Fonds de recherche du Québec—Santé (FRQS) Chercheurs-boursiers award given with Parkinson Quebec, and is a Parkinson Canada New Investigator awardee. The access to the McGill participants for this research has been made possible in part thanks to the Quebec Parkinson's Network (<http://rpq-qpn.ca/en/>). NIH [R01AG054008, R01NS095252, R01AG060961, R01AG060961] to JFC, the Rainwater Charitable Foundation/Tau Consortium (JFC), Genentech/Roche, and an Alexander Saint-Amand Scholarship (JFC). This work was supported in part by the Intramural Research Programs of the National Institute of Neurological Disorders and Stroke (NINDS), the National Institute on Aging (NIA), and the National Institute of Environmental Health Sciences both part of the National Institutes of Health, Department of Health and Human Services: project numbers 1ZIA-NS003154, Z01-AG000949-02 and Z01-ES101986. BrightFocus Foundation, Association for Frontotemporal Degeneration, CurePSP, Rainwater Charitable Foundation, National Institutes of Health, Michael J. Fox Foundation for Parkinson's Research, Canadian Consortium on Neurodegeneration in Aging, Canada First Research Excellence Fund, Fonds de Recherche du Québec—Santé

Availability of data and materials

All aligned read counts and FASTQ files for *LRRK37A*-overexpressing HEK293T cells will be deposited to the Gene Expression Omnibus once the manuscript is accepted for publication.

Declarations

Declarations

Ethical Approval and Consent to Participate

Not applicable.

Consent for publication

All authors read and approved the final manuscript

Competing interests

AMG: Scientific advisory board (SAB) for Denali Therapeutics (2015–2018), SAB for Pfizer (2019), SAB for Genentech, consultant for GSK, AbbVie, Biogen and Eisai. All other authors declare no competing interests.

Author details

¹Department of Genetics and Genomic Sciences, Icahn School of Medicine at Mount Sinai, New York, NY, USA. ²Ronald M. Loeb Center for Alzheimer's Disease, Icahn School of Medicine at Mount Sinai, New York, NY, USA. ³Laboratory of Neurogenetics, National Institute on Aging, National Institutes of Health, Bethesda, MD, USA. ⁴Department of Human Genetics, McGill University, Montréal, Québec, Canada. ⁵The Neuro (Montreal Neurological Institute-Hospital), McGill University, Montréal, Québec, Canada. ⁶Department of Neurology

and Neurosurgery, McGill University, Montréal, Québec, Canada. ⁷Department for Neurodegenerative Diseases, Hertie Institute for Clinical Brain Research, University of Tübingen, Tübingen, Germany. ⁸German Center for Neurodegenerative Diseases (DZNE), Tübingen, Germany. ⁹Institute of Clinical Medicine, Department of Neurology, University of Oulu, Oulu, Finland. ¹⁰Department of Neurology and Medical Research Center, Oulu University Hospital, Oulu, Finland. ¹¹Alzheimer's Disease and CTE Center, Boston University, Boston University School of Medicine, Boston, MA, USA. ¹²Department of Neurology, Boston University School of Medicine, Boston, MA, USA. ¹³VA Boston Healthcare System, 150 S. Huntington Avenue, Boston, MA, USA. ¹⁴Department of Pathology and Laboratory Medicine, Boston University School of Medicine, Boston, MA, USA. ¹⁵Department of Psychiatry, Washington University in St. Louis, St. Louis, MO, USA. ¹⁶Department of Neurology, Fresco Institute for Parkinson's and Movement Disorders, New York University Langone, New York, NY, USA. ¹⁷Department of Neurosurgery, Icahn School of Medicine at Mount Sinai, New York, NY, USA. ¹⁸Center for Neuromodulation, Icahn School of Medicine at Mount Sinai, New York, NY, USA. ¹⁹Icahn Genomics Institute, Icahn School of Medicine at Mount Sinai, New York, NY, USA. ²⁰Institute for Exposomic Research, Icahn School of Medicine at Mount Sinai, New York, NY, USA. ²¹Department of Psychiatry, Icahn School of Medicine at Mount Sinai, New York, NY, USA. ²²IPDGC Authors and Affiliations in Supplementary Material 2, New York, NY, USA. ²³Estelle and Daniel Maggin Department of Neurology, Icahn School of Medicine at Mount Sinai, New York, NY, USA. ²⁴Department of Pathology, Icahn School of Medicine at Mount Sinai, New York, NY, USA.

Received: 23 September 2021 Accepted: 21 June 2022

Published online: 15 July 2022

References

- Jun G, Ibrahim-Verbaas CA, Vronskaya M, Lambert J-C, Chung J, Naj AC. A Novel Alzheimer Disease Locus Located Near the Gene Encoding Tau Protein. *2016*;21:108–17.
- Kouri N, Ross OA, Dombroski B, et al. Genome-wide association study of corticobasal degeneration identifies risk variants shared with progressive supranuclear palsy. *Nat Commun*. 2015;6:1–7.
- Höglinger GU, Melhem NM, Dickson DW, et al. Identification of common variants influencing risk of the tauopathy progressive supranuclear palsy. *Nat Genet*. 2011;43:699–705.
- Chen JA, Chen Z, Won H, et al. Joint genome-wide association study of progressive supranuclear palsy identifies novel susceptibility loci and genetic correlation to neurodegenerative diseases. *Mol Neurodegener*. 2018;13:1–11.
- Pastor P, Ezquerra M, Perez JC, et al. Novel Haplotypes in 17q21 Are Associated with Progressive Supranuclear Palsy. *Ann Neurol*. 2004;56:249–58.
- Bandrés-ciga S, Ryan T, Javier F, et al. Genome-wide assessment of Parkinson's disease in a Southern Spanish population. *Neurobiol Aging*. 2016;45(213):e3-213.e9.
- Desikan RS, Schork AJ, Wang Y, et al. Genetic overlap between Alzheimer's disease and Parkinson's disease at the MAPT locus. *Mol Psychiatry* 2015;20(12):1588–95.
- Nalls MA, Pankratz N, Lill CM, et al. Large-scale meta-analysis of genome-wide association data identifies six new risk loci for Parkinson's disease. *Nat Genet*. 2014;46:989–93.
- Bandrés-Ciga S, Ahmed S, Sabir MS, et al. The genetic architecture of Parkinson disease in Spain: characterizing population-specific risk, differential haplotype structures, and providing etiologic insight. *Mov Disord*. 2019. <https://doi.org/10.1101/609016>.
- Nalls MA, Blauwendraat C, Vallerga CL, et al. Identification of novel risk loci, causal insights, and heritable risk for Parkinson's disease: a meta-analysis of genome-wide association studies. *Lancet Neurol*. 2019;18(12):1091–102.
- Galvin JE, Pollack J, Morris JC. Clinical phenotype of Parkinson disease dementia. *Neurology*. 2006;67:1605–12.
- Aarsland D, Zaccari J, Brayne C. A Systematic Review of Prevalence Studies of Dementia in Parkinson's Disease. *Mov Disord*. 2005;20:1255–63.
- Massano J, Bhatia KP. Clinical Approach to Parkinson's Disease: Features, Diagnosis, and Principles of Management. *Cold Spring Harb Perspect Med*. 2012;2(6):1–15.
- Spillantini MG, Schmidt ML, Lee VM-Y, Trojanowski JQ, Jakes R, Goedert M. alpha-Synuclein in Lewy bodies. *Nature*. 1997;388:839–40.
- Dickson DW. Neuropathology of Parkinson Disease. *Parkinsonism Relat Disord*. 2018;46:1–11.
- Zhang X, Gao F, Wang D, et al. Tau Pathology in Parkinson's Disease. *Front Neurol*. 2018;9:1–7.
- Espay AJ, Vizcarra JA, Marsili L, et al. Revisiting protein aggregation as pathogenic in sporadic Parkinson and Alzheimer diseases. *Neurology*. 2019;92:329–37.
- Zabetian CP, Hutter CM, Factor S, et al. Association Analysis of MAPT H1 Haplotype and Subhaplotypes in Parkinson's Disease. *Ann Neurol*. 2007;62:137–44.
- Vandrovicova J, Pittman AM, Malzer E, et al. Association of MAPT haplotype-tagging SNPs with sporadic Parkinson's disease. *Neurobiol Aging*. 2009;30:1477–82.
- Boettger LM, Handsaker RE, Zody MC, McCarroll SA. Structural haplotypes and recent evolution of the human 17q21.31 region. *Nat Genet*. 2012;44:881–5.
- Steinberg KM, Antonacci F, Sudmant PH, et al. Structural diversity and African origin of the 17q21.31 inversion polymorphism. *Nat Publ Gr*. 2012;44:872–80.
- Brück D, Wenning GK, Stefanova N, Fellner L. Glia and alpha-synuclein in neurodegeneration: A complex interaction. *Neurobiol Dis*. 2016;85:262–74.
- di Domenico A, Carola G, Calatayud C, et al. Patient-Specific iPSC-Derived Astrocytes Contribute to Non-Cell-Autonomous Neurodegeneration in Parkinson's Disease. *Stem Cell Reports*. 2019;12:213–29.
- Booth HDE, Hirst WD, Wade-Martins R. The Role of Astrocyte Dysfunction in Parkinson's Disease Pathogenesis. *Trends Neurosci*. 2017;40:358–70.
- Sonninen TM, Hämäläinen RH, Koskivi M, et al. Metabolic alterations in Parkinson's disease astrocytes. *Sci Rep* 2020; 10. DOI:<https://doi.org/10.1038/s41598-020-71329-8>.
- Wakabayashi K, Hayashi S, Yoshimoto M, Kudo Y, Takahashi H. NACP alphasynuclein-positive filamentous inclusions. *Acta Neuropathol*. 2000;99:14–20.
- Song YJC, Halliday GM, Holton JL, et al. Degeneration in different parkinsonian syndromes relates to astrocyte type and astrocyte protein expression. *J Neuropathol Exp Neurol*. 2009;68:1073–83.
- Braak H, Sastre M, Del Tredici K. Development of alpha-synuclein immunoreactive astrocytes in the forebrain parallels stages of intraneuronal pathology in sporadic Parkinson's disease. *Acta Neuropathol*. 2007;114:231–41.
- Lee HJ, Suk JE, Patrick C, et al. Direct transfer of alpha-synuclein from neuron to astroglia causes inflammatory responses in synucleinopathies. *J Biol Chem*. 2010;285:9262–72.
- Pittman A, Myers A, Abou-Sleiman P, et al. Linkage disequilibrium fine mapping and haplotype association analysis of the tau gene in progressive supranuclear palsy and corticobasal degeneration. *J Med Genet*. 2005;42:837–46.
- Rothhammer V, Quintana FJ. Control of autoimmune CNS inflammation by astrocytes. *Semin Immunopathol*. 2015;37:625–38.
- Zhou Y, Zhu Y. Important role of the IL-32 inflammatory network in the host response against viral infection. *Viruses*. 2015;7:3116–29.
- Mathys H, Davila-Velderrain J, Peng Z, et al. Single-cell transcriptomic analysis of Alzheimer's disease. *Nature*. 2019;570:332–7.
- Smajic S, Prada-Medina CA, Landoulsi Z, et al. Single-cell sequencing of the human midbrain reveals glial activation and a neuronal state specific to Parkinson's disease. *Brain*. 2021. <https://doi.org/10.1101/2020.09.28.20202812>.
- Donnelly MP, Paschou P, Grigorenko E, et al. The Distribution and Most Recent Common Ancestor of the 17q21 Inversion in Humans. *Am J Hum Genet*. 2010;86:161–71.
- Sánchez-Juan P, Moreno S, de Rojas I, et al. The MAPT H1 Haplotype Is a Risk Factor for Alzheimer's Disease in APOE ε4 Non-carriers. *Front Aging Neurosci*. 2019;11:1–9.
- Gayán J, Galan JJ, González-Pérez A, et al. Genetic Structure of the Spanish Population. *BMC Genomics* 2010; 11. DOI:<https://doi.org/10.1186/1471-2164-11-326>.
- Coupland KG, Kim WS, Halliday GM, Hallupp M, Dobson-Stone C, Kwok JBJ. Role of the long non-coding RNA MAPT-AS1 in regulation of microtubule associated protein tau (MAPT) expression in Parkinson's disease. *PLoS ONE*. 2016;11:1–14.

39. Simone R, Javad F, Emmett W, et al. MIR-NATs repress MAPT translation and aid proteostasis in neurodegeneration. *Nature*. 2021;594:117–23.
40. Soutar MPM, Melandri D, Annuario E, et al. Regulation of mitophagy by the NSL complex underlies genetic risk for Parkinson's disease at Chr16q11.2 and on the MAPT H1 allele. *bioRxiv* 2020. DOI:<https://doi.org/10.1101/2020.01.06.896241>.
41. Giannuzzi G, Siswara P, Malig M, et al. Evolutionary dynamism of the primate LRRC37 gene family. *Genome Res*. 2013;23:46–59.
42. Zody MC, Jiang Z, Fung H-C, et al. Evolutionary toggling of the MAPT 17q21.31 inversion region. *Nat Genet*. 2008;40:1076–83.
43. Falola MI, Wiener HW, Wineinger NE, et al. Genomic Copy Number Variants: Evidence for Association with Antibody Response to Anthrax Vaccine Adsorbed. *PLoS One* 2013; 8. DOI:<https://doi.org/10.1371/journal.pone.0064813>.
44. Miklossy J, Doudet DD, Schwab C, Yu S, McGeer EG, McGeer PL. Role of ICAM-1 in persisting inflammation in Parkinson disease and MPTP monkeys. *Exp Neurol*. 2006;197:275–83.
45. Koprach JB, Reske-Nielsen C, Mithal P, Isacson O. Neuroinflammation mediated by IL-1 β increases susceptibility of dopamine neurons to degeneration in an animal model of Parkinson's disease. *J Neuroinflammation*. 2008;5:1–12.
46. Zhang Y, Sloan SA, Clarke LE, et al. Purification and characterization of progenitor and mature human astrocytes reveals transcriptional and functional differences with mouse. *Neuron*. 2016;89:37–53.
47. Huang A, Martin ER, Vance JM, Cai X. Detecting genetic interactions in pathway-based genome-wide association studies. *Genet Epidemiol*. 2014;38:300–9.
48. Kong Y, Liang X, Liu L, et al. High throughput sequencing identifies MicroRNAs mediating α -synuclein toxicity by targeting neuroactive-ligand receptor interaction pathway in early stage of Drosophila Parkinson's disease model. *PLoS ONE*. 2015;10:1–24.
49. Fallon J, Reid S, Kinyamu R, et al. In vivo induction of massive proliferation, directed migration, and differentiation of neural cells in the adult mammalian brain. *Proc Natl Acad Sci U S A*. 2000;97:14686–91.
50. Lee HJ, Kim C, Lee SJ. Alpha-synuclein stimulation of astrocytes: Potential role for neuroinflammation and neuroprotection. *Oxid Med Cell Longev*. 2010;3:283–7.
51. Wang C, Yang T, Liang M, Xie J, Song N. Astrocyte dysfunction in Parkinson's disease: from the perspectives of transmitted α -synuclein and genetic modulation. *Transl Neurodegener*. 2021;10:1–17.
52. Mena MA, García De Yébenes J. Glial cells as players in parkinsonism: The 'good', the 'bad', and the 'mysterious' glia. *Neuroscientist*. 2008;14:544–60.
53. Purcell S, Neale B, Todd-Brown K, et al. PLINK: A Tool Set for Whole-Genome Association and Population-Based Linkage Analyses. *Am J Hum Genet*. 2007;81:559–75.
54. Consortium TIH. The International HapMap Project. *Nature*. 2003;426:789–96.
55. Patterson N, Price AL, Reich D. Population structure and eigenanalysis. *PLoS Genet*. 2006;2:2074–93.
56. Das S, Forer L, Schonherr S, et al. Next-generation genotype imputation service and methods Sayantan. 2016;48:1284–7.
57. Lumley T. *rmeta: Meta-Analysis*. R package version 3.0. 2018; : <https://CRAN.R-project.org/package=rmeta>.
58. Barrett JC, Fry B, Maller J, Daly MJ. Haploview: analysis and visualization of LD and haplotype maps. *Bioinformatics*. 2005;21:263–5.
59. Gabriel SB, DeFolice M, Rotimi C, et al. The structure of haplotype blocks in the human genome. *Science*. 2002;296(80-):2225–9.
60. Aragon TJ. *epitools: Epidemiology Tools*. R package version 0.5–10.1; 2020. <https://CRAN.R-project.org/package=epitools>.
61. Heckman MG, Brennan RR, Labbé C, et al. Association of MAPT Subhaplotypes With Risk of Progressive Supranuclear Palsy and Severity of Tau Pathology. *JAMA Neurol*. 2019;76(6):1–8.
62. Katz Y, Wang ET, Airolidi EM, Burge CB. Analysis and design of RNA sequencing experiments for identifying isoform regulation. *Nat Methods*. 2010;7:1009–15.
63. Karch CM, Kao AW, Karydas A, et al. A Comprehensive Resource for Induced Pluripotent Stem Cells from Patients with Primary Tauopathies. *Stem cell reports*. 2019;13:1–17.
64. Hoffman GE, Hartley BJ, Flaherty E, et al. Transcriptional signatures of schizophrenia in hiPSC-derived NPCs and neurons are concordant with post-mortem adult brains. *Nat Commun* 2017; 8. DOI:<https://doi.org/10.1038/s41467-017-02330-5>.
65. Bowles KR, Julia TCW, Qian L, Jadow BM, Goate AM. Reduced variability of neural progenitor cells and improved purity of neuronal cultures using magnetic activated cell sorting. *PLoS ONE*. 2019;14:1–18.
66. Tcw J, Wang M, Pimenova AA, et al. An Efficient Platform for Astrocyte Differentiation from Human Induced Pluripotent Stem Cells. *Stem Cell Reports*. 2017;9:600–14.
67. Tcw J, Wang M, Pimenova AA, et al. An Efficient Platform for Astrocyte Differentiation from Human Induced Pluripotent Stem Cells. *Stem Cell Reports*. 2017;9:600–14.
68. Patro R, Duggal G, Love MI, Irizarry RA, Kingsford C. Salmon: fast and bias-aware quantification of transcript expression using dual-phase inference. *Nat Methods*. 2017;14:417.
69. Ritchie ME, Phipson B, Wu D, et al. limma powers differential expression analyses for RNA-seq and microarray studies. *Nucleic Acids Res*. 2015;43: e47.
70. Subramanian A, Subramanian A, Tamayo P, et al. Gene set enrichment analysis: a knowledge-based approach for interpreting genome-wide expression profiles. *Proc Natl Acad Sci U S A*. 2005;102:15545–50.
71. Reimand J, Kull M, Peterson H, Hansen J, Vilo J. G:Profiler-a web-based toolset for functional profiling of gene lists from large-scale experiments. *Nucleic Acids Res*. 2007;35:1–8.
72. Raudvere U, Kolberg L, Kuzmin I, et al. g:Profiler: a web server for functional enrichment analysis and conversions of gene lists (2019 update). *Nucleic Acids Res*. 2019;47:1–8.
73. Shannon P, Markiel A, Ozier O, et al. Cytoscape: A Software Environment for Integrated Models of Biomolecular Interaction Networks. *Genome Res*. 2003;13(11):2498–504.
74. Merico D, Isserlin R, Stueker O, Emili A, Bader GD. Enrichment map: A network-based method for gene-set enrichment visualization and interpretation. *PLoS One* 2010; 5. DOI:<https://doi.org/10.1371/journal.pone.0013984>.
75. Stuart T, Butler A, Hoffman P, et al. Comprehensive Integration of Single-Cell Data. *Cell*. 2019;177:1888–1902.e21.
76. Butler A, Hoffman P, Smibert P, Papalexi E, Satija R. Integrating single-cell transcriptomic data across different conditions, technologies, and species. *Nat Biotechnol* 2018; 36. DOI:<https://doi.org/10.1038/nbt.4096>.
77. Hafemeister C, Satija R. Normalization and variance stabilization of single-cell RNA-seq data using regularized negative binomial regression. *Genome Biol*. 2019;20:1–15.
78. McInnes L, Healy J, Melville J. UMAP: Uniform manifold approximation and projection for dimension reduction. *arXiv:1802.03426*;2018.
79. Wolf F, Angerer P, Theis F. SCANPY: large-scale single-cell gene expression data analysis. *Genome Biol*. 2018;19. <https://doi.org/10.1111/1462-2920.13787>.

Publisher's Note

Springer Nature remains neutral with regard to jurisdictional claims in published maps and institutional affiliations.

Ready to submit your research? Choose BMC and benefit from:

- fast, convenient online submission
- thorough peer review by experienced researchers in your field
- rapid publication on acceptance
- support for research data, including large and complex data types
- gold Open Access which fosters wider collaboration and increased citations
- maximum visibility for your research: over 100M website views per year

At BMC, research is always in progress.

Learn more biomedcentral.com/submissions

